

# Rayleigh Scattering and Microwave Background Fluctuations

Qingjuan Yu, David N. Spergel<sup>1</sup> & Jeremiah P. Ostriker

Department of Astrophysical Sciences, Princeton University, Princeton, NJ 08544

## ABSTRACT

During the recombination epoch, cosmic background photons couple not only to free electrons through Thompson scattering, but also to the neutral hydrogen through Rayleigh scattering. This latter is  $\sim 2\%$  effect for photons near the peak of the photon energy distribution at  $z = 800$  and a  $\sim 0.2\%$  effect at  $z = 1100$ . Including Rayleigh scattering in the calculation reduces Silk damping at fixed redshift, alters the position of the surface of last scattering and alters the propagation of acoustic waves. We estimate the amplitude of these effects. For the *Microwave Anisotropy Probe (MAP)*, Rayleigh scattering increases the anisotropy spectrum by 0.1% at the most. For the highest frequencies of the *Planck Surveyor*, the effects of Rayleigh scattering are much more dramatic (decreasing the anisotropy spectrum by 3% at  $\nu \sim 550\text{GHz}$  and  $l \sim 1000$ ). The relative difference between the spectra of low and high frequencies is imposed by an oscillation with a function of multipole  $l$  and the oscillation amplitude is up to 0.5% between 100 and 550 GHz. Rayleigh scattering also slows the decoupling between radiation and matter, but the effect is undetectably small.

## 1. Introduction

With the upcoming launch of the *Microwave Anisotropy Probe (MAP)*<sup>2</sup> in 2001 and the *Planck Surveyor*<sup>3</sup> in 2007, the study of the cosmic microwave background (CMB) fluctuations is about to enter a new epoch. These satellites will characterize the statistical properties of the microwave background at better than the 1% level. This dramatic improvement in experimental capabilities demands that theorists attempt to achieve this level of accuracy in their calculations. Otherwise, systematic errors in the theoretical calculations will lead

---

<sup>1</sup>W.M. Keck Distinguished Visiting Professor of Astrophysics, Institute for Advanced Study, Princeton, NJ 08540

<sup>2</sup>For details, see <http://map.gsfc.nasa.gov>.

<sup>3</sup>For details, see <http://astro.estec.esa.nl/Planck/>.

to systematic errors in our interpretation. Over the past several years, several corrections to the CMB spectrum have been identified that systematically alter the predictions of a given model at the 1% level (Hu et al. 1995; Gnedin & Gnedin 1998; Seager, Sasselov & Scott 1999). Without these corrections, theoretical systematic biases could be as important as experimental error. This paper explores another possible source of systematic error: neglecting Rayleigh scattering in estimates of the CMB fluctuation spectrum.

In their seminal paper, Peebles & Yu (1970) note that Rayleigh scattering accounts for a few percent of the opacity near decoupling. To simplify their analysis, they ignore it and include only Thompson scattering in their calculation. Most subsequent analytical and numerical work has also included only Thompson scattering. This approximation makes the amplitude of cosmic microwave background fluctuations a simple function of frequency and greatly simplifies the equations. Hannestad (2001) considers the effect of Rayleigh scattering; however, since he does not do a frequency-dependent calculation, he significantly underestimates its importance.

In this paper, we estimate the effects of Rayleigh scattering on microwave background fluctuations. Our calculation begins with the analytical approach of Peebles (1980) and Hu & Sugiyama (1995): we treat the photon-baryon fluid as tightly coupled through the surface of last scattering. While this approach is not exact, it enables us to estimate and identify the effects of Rayleigh scattering. In section 2, we discuss the propagation of acoustic waves in the baryon-photon fluid. The additional opacity source reduces photon diffusion and also leads to a frequency dependence in the phase of the acoustic wave. In section 3, we identify four different observational effects. While some of these effects are important only at high frequencies, the suppression of Silk damping leads to observationally significant changes in the Rayleigh-Jeans regime. In section 4, we check our analytical estimates with a full numerical integration of the full Boltzmann equations using a modified version of CMBFAST. Section 5 concludes. In this paper, if not specified, the speed of light is set to be 1.

## 2. Acoustic Wave Propagation

Rayleigh scattering adds an additional source of opacity to photon propagation:

$$\lambda^{-1}(\nu) = n_e \sigma_T + n_H \sigma_T \left( \frac{\nu}{\nu_{eff}} \right)^4, \quad (1)$$

where  $n_e$  is the electron density,  $n_H$  is the neutral hydrogen density,  $\sigma_T$  is the Thompson cross-section, and

$$\nu_{eff}^{-2} \equiv \sum_{j=2}^{\infty} f_{1j}/(\nu_{1j}^2 - \nu^2) \simeq \sum_{j=2}^{\infty} f_{1j} \nu_{1j}^{-2} \simeq (0.95cR_A)^{-2}, \quad \text{for } \nu \ll \nu_{12}, \quad (2)$$

where  $f_{1j}$  is the Lyman series oscillator strength,  $\nu_{1j}$  is the Lyman series frequency,  $c$  is the speed of light and  $R_A$  is the Rydberg constant of hydrogen atoms (see Lang 1999, equation [1.306], and the oscillator strength in equation [2.118] and references therein). Looking at equation (1) and ignoring the frequency dependence, one sees that, roughly speaking, addition of Rayleigh scattering corresponds to an increasing  $n_e$  or  $\Omega_b h^2$  (where  $\Omega_b$  is the baryon density in units of critical density and the Hubble constant  $H_0 = 100h \text{ km s}^{-1} \text{ Mpc}^{-1}$ ), which will be seen to be true at low frequencies (i.e., the increasing of anisotropy spectra at  $\nu \lesssim 150 \text{ GHz}$ ) in §4. Other atomic and molecular processes are unimportant: the abundances of  $\text{H}_2$ , HD and other molecules are low in the early universe (Stancil, Lepp & Dalgarno 1998) and neither He or  $\text{H}^-$  are significant sources of opacity at the relevant frequencies. The fractional abundance of hydrogen in the  $n = 2$  state peaks at  $10^{-13}$  just prior to decoupling (Stancil, Lepp & Dalgarno 1998), so Balmer lines are not a significant source of opacity.

In this section, we explore the effects of a *frequency dependent* cross-section on acoustic wave propagation. Assuming that the radiation is unpolarized, we begin by expanding the microwave background fluctuations into a smooth unperturbed piece  $f^{(0)}(\nu) = [\exp(h_P \nu / k_B T) - 1]^{-1}$  (where  $h_P$  is the Planck constant,  $k_B$  is the Boltzmann constant,  $\nu$  is the comoving frequency and  $T$  is the present temperature), and, in the conformal Newtonian gauge, a perturbation piece that obeys the linear collisional Boltzmann equation (Wilson & Silk 1981; Bond & Efstathiou 1984; Dodelson & Jubas 1995; Hu & Sugiyama 1995):

$$\frac{\partial f^{(1)}(\nu, k, \mu)}{\partial \eta} + ik\mu \left[ f^{(1)}(\nu, k, \mu) - \frac{\partial f^{(0)}(\nu)}{\partial \ln \nu} \Psi(k, \eta) \right] = \frac{\partial f^{(0)}(\nu)}{\partial \ln \nu} \frac{\partial \Phi(k, \eta)}{\partial \eta} + \frac{a}{a_0} \frac{1}{\lambda[(1 + z(\eta))\nu]} \times \left[ f_0^{(1)}(\nu, k) + \frac{1}{2} f_2^{(1)}(\nu, k) P_2(\mu) - f^{(1)}(\nu, k, \mu) - \frac{\partial f^{(0)}(\nu)}{\partial \ln \nu} \mu u_b(k) \right], \quad (3)$$

where  $\mu = \hat{\mathbf{k}} \cdot \hat{\mathbf{n}}$ ,  $\hat{\mathbf{k}}$  is the comoving wavevector of the perturbation,  $\hat{\mathbf{n}}$  is the unit vector in the direction of propagation,  $k = |\hat{\mathbf{k}}|$  is the comoving wavenumber,  $u_b$  is the baryon velocity,  $\eta$  is the conformal time and  $z(\eta)$  is the redshift at  $\eta$ . The  $a$  is the scale factor and its value at the present time is  $a_0$ .  $\Psi$  and  $\Phi$  are the Newtonian potential and the perturbation to the intrinsic spatial curvature. The photon distribution function is expanded in Legendre polynomials:

$$f^{(1)}(\nu, k, \mu) = \sum_{l=0}^{\infty} f_l^{(1)}(\nu, k) (2l + 1) P_l(\mu). \quad (4)$$

Ignoring changes in  $R(=3\rho_\gamma/4\rho_b$ , where  $\rho_\gamma$  and  $\rho_b$  are the radiation density and baryon density respectively) and terms involving  $\Phi$  and  $\Psi$ , a moment expansion of equation (3) gives (e.g., Hu & Sugiyama 1996):

$$\begin{aligned}\dot{f}_0^{(1)}(\nu, k) &= -ikf_1^{(1)}(\nu, k), \\ \dot{f}_1^{(1)}(\nu, k) &= -\frac{ik}{3} \left[ f_0^{(1)}(\nu, k) + 2f_2^{(1)}(\nu, k) \right] - \frac{a}{a_0} \frac{1}{\lambda[(1+z(\eta))\nu]} \left[ f_1^{(1)}(\nu, k) + \frac{1}{3} \frac{\partial f^{(0)}(\nu)}{\partial \ln \nu} u_b(k) \right], \\ \dot{f}_2^{(1)}(\nu, k) &= -\frac{2}{5}ikf_1^{(1)}(\nu, k) - \frac{a}{a_0} \frac{1}{\lambda[(1+z(\eta))\nu]} \left[ f_2^{(1)}(\nu, k) \right],\end{aligned}\quad (5)$$

where we have truncated the expansion beyond the second moment and ignored the angular dependence of Compton and Rayleigh scattering. Overdots represent derivatives to the conformal time  $\eta$ . The baryon velocity obeys the familiar mass and momentum conservation equations:

$$\begin{aligned}\dot{\delta}_b(k) &= iku_b(k), \\ \rho_b \dot{u}_b(k) &= \frac{a}{a_0} \int \frac{8\pi h_P \nu^3 d\nu}{\lambda[(1+z(\eta))\nu]} \left[ f_1^{(1)}(\nu, k) + \frac{\partial f^{(0)}(\nu)}{\partial \ln \nu} \frac{u_b(k)}{3} \right] - i\rho_b c_b^2 k \delta_b(k),\end{aligned}\quad (6)$$

where  $\delta_b$  is the baryon over-density and  $c_b$  is the baryon sound speed. This equation explicitly allows for the extra photon drag due to Compton and Rayleigh scattering, and, consequently, for the slightly later momentum decoupling and lower amplitude of the baryon fluctuations. But the heating on the baryon due to the extra photon drag of Rayleigh scattering can be neglected because of the small relevant ratio for comparing Rayleigh and Compton heating  $\sim (m_e/m_p)[\langle \lambda^T/\lambda(\nu) \rangle - 1] \sim 10^{-5}$ , where  $m_e/m_p$  is the electron mass to proton mass ratio,  $\langle \lambda^T/\lambda(\nu) \rangle (= \lambda^T/\tilde{\lambda}(\eta)$ , see equation 7) is the mean free path ratio of photons without Rayleigh scattering to photons with Rayleigh scattering, which can be estimated from Figure 1 later. We assume that the baryon sound velocity is small and ignore its pressure.

We define a momentum weighted mean free path, which is equivalent to the Rosseland mean opacity in stellar atmospheres:

$$\begin{aligned}\frac{1}{\tilde{\lambda}(\eta)} &= \int \frac{\nu^3 d\nu}{\lambda[(1+z(\eta))\nu]} \frac{\partial f^{(0)}(\nu)}{\partial \ln \nu} \Big/ \int \nu^3 d\nu \frac{\partial f^{(0)}(\nu)}{\partial \ln \nu} \\ &= -\frac{1}{4\rho_\gamma} \int \frac{8\pi h_P \nu^3 d\nu}{\lambda[(1+z(\eta))\nu]} \frac{\partial f^{(0)}(\nu)}{\partial \ln \nu}.\end{aligned}\quad (7)$$

Following Peebles (1980), we look for solutions proportional to  $\exp(i \int \omega(k, \eta))$ . We expand the solutions in  $\delta\lambda = (\lambda[(1+z(\eta))\nu] - \tilde{\lambda}(\eta))$

$$f_1^{(1)}(\nu, k) = A(k) \frac{\partial f^{(0)}(\nu)}{\partial \ln \nu} [1 + b(k)\delta\lambda + o(\delta\lambda)] \exp \left[ - \int i\omega(k, \eta) d\eta \right]. \quad (8)$$

Substituting this back into equation (3), we find

$$\begin{aligned} f_0^{(1)}(\nu, k) &= \frac{-k}{\omega(k)} f_1^{(1)}(\nu, k); \\ f_2^{(1)}(\nu, k) &= -\frac{2}{5} ik\lambda[(1+z(\eta))\nu] f_1^{(1)}(\nu, k); \end{aligned} \quad (9)$$

and (6):

$$u_b(k) = -3A(k) \frac{1}{1 - i\omega(k)R\tilde{\lambda}} \exp \left[ - \int i\omega(k, \eta) d\eta \right]. \quad (10)$$

We can insert equations (9) and (10) back in equation (5). Solving the equations for the frequency to second order in  $\tilde{\lambda}$  yields,

$$\omega(k) = c_s k - i\gamma k^2 \tilde{\lambda}, \quad (11)$$

where

$$c_s^2 = \frac{1}{3} \frac{1}{1+R}; \quad (12)$$

$$\gamma = \frac{R^2 + 4(1+R)/5}{6(1+R)^2}. \quad (13)$$

The inclusion of Rayleigh scattering has altered the dispersion relation by reducing  $\tilde{\lambda}$  due to the second term in equation (1).

The temperature perturbation is defined by  $\delta T/T \equiv \Theta(\nu, k, \mu) = -f^{(1)}(\nu, k, \mu)/\frac{\partial f^{(0)}(\nu)}{\partial \ln \nu}$  and can be expanded in Legendre polynomials  $\Theta(\nu, k, \mu) = \sum_{l=0} \Theta_l(\nu, k) (2l+1) P_l(\mu)$ .

Thus, from equation (3), we have the evolution of temperature perturbation:

$$\dot{\Theta} + ik\mu(\Theta + \Psi) = -\dot{\Phi} + \frac{a}{a_0} \frac{1}{\lambda[(1+z(\eta))\nu]} [\Theta_0 - \Theta + \frac{1}{2} \Theta_2 P_2(\mu) + \mu u_b]. \quad (14)$$

If we ignore the angular dependence of Compton scattering, equation (14) has the solution:

$$(\Theta + \Psi)(\nu, k, \mu, \eta_0) = \int_0^{\eta_0} [-(\Theta_0 + \Psi + \mu u_b) \dot{\tau}(\nu, \eta, \eta_0) - \dot{\Phi} + \dot{\Psi}] e^{-\tau(\nu, \eta, \eta_0)} e^{ik\mu(\eta - \eta_0)} d\eta, \quad (15)$$

where  $\eta_0$  is the present epoch and  $\tau(\nu, \eta_1, \eta_2) \equiv \int_{\eta_1}^{\eta_2} \frac{a}{a_0} \frac{1}{\lambda[(1+z(\eta))\nu]} d\eta$ .

Taking the multipole moments of equation (15) and setting  $u_b = 3\Theta_1$ , we have for  $l \geq 2$  (Hu & Sugiyama 1995),

$$\begin{aligned} \Theta_l(\nu, k, \eta_0) &\approx (\Theta_0 + \Psi)(\eta_*) (-i)^l j_l(k\Delta\eta_*) + \frac{3}{2l+1} (-i)^{l-1} \Theta_1(\eta_*) [l j_{l-1}(k\Delta\eta_*) \\ &\quad - (l+1) j_{l+1}(k\Delta\eta_*)] + (-i)^l \int_{\eta_*}^{\eta_0} (\dot{\Psi} - \dot{\Phi}) j_l(k\Delta\eta) d\eta, \end{aligned} \quad (16)$$

where  $\Delta\eta \equiv \eta_0 - \eta$ ,  $\Delta\eta_* \equiv \eta_0 - \eta_*(\nu)$ ,  $\eta_0$  is the present epoch and  $\eta_*(\nu)$  is the epoch at the last scattering. The fluctuations on the last scattering surface are obtained from  $(\Theta_0 + \Psi)(\eta_*) = (\hat{\Theta}_0 + \Psi)(\eta_*)D(k, \nu)$  and  $\Theta_1(\eta_*) = \hat{\Theta}_1(\eta_*)D(k, \nu)$ , where  $D(k, \nu)$  is the damping factor (see its definition in §3.1). The undamped WKB solution  $\hat{\Theta}_0(\eta)$  and  $\hat{\Theta}_1(\eta)$ , as well as the potential  $\Psi(\eta)$  and  $\Phi(\eta)$ , can be obtained from the Appendix in Hu & Sugiyama (1995). They are all assumed not to be affected by Rayleigh scattering here, which is confirmed to be reasonable by the consistency between our analytical and numerical results in §4.

Integrating over all  $k$  modes of the perturbation, we have the power spectrum of the auto-correlation function:

$$\frac{1}{4\pi}C_l(\nu) = \frac{V}{2\pi^2} \int \frac{dk}{k} k^3 |\Theta_l(\nu, k, \eta_0)|^2. \quad (17)$$

### 3. Observable Effects

Rayleigh scattering produces several observable effects. We begin our discussion with effects that are detectable in the Rayleigh-Jeans part of the spectrum and then turn to effects that are detectable only in the Wien tail.

#### 3.1. Suppression of Silk Damping

Our treatment of Silk damping follows the analytical approach developed by Hu & Sugiyama (1995). At a given wavenumber, the amplitude of Silk damping is the integrated photon diffusion length:

$$k_D^{-2}(\eta) = \int_0^\eta \gamma \tilde{\lambda}(\eta') d\eta'. \quad (18)$$

Since Rayleigh scattering reduces the photon-diffusion length, it reduces the amplitude of Silk damping. The damping factor at a given wavenumber is weighted by the photon visibility function:

$$D(k, \nu) \equiv \int_0^{\eta_0} d\eta \mathcal{V}(\nu, \eta) \exp\left[-\frac{k^2}{k_D^2(\eta)}\right], \quad (19)$$

where the  $\mathcal{V}(\eta)$  is the photon visibility function

$$\mathcal{V}(\nu, \eta) \equiv -\dot{\tau}(\nu, \eta, \eta_0) \exp[-\tau(\nu, \eta)], \quad (20)$$

where  $\tau$  is the photon mean free path (Figure 1). Figure 2 shows the damping factor as a function of  $k$  with and without Rayleigh scattering for a flat vacuum-dominated universe

with  $\Omega_m = 0.35$ ,  $h = 0.65$  and  $\Omega_b = 0.05$  (where  $\Omega_m$  is the mass density in units of the critical density).

At low frequencies, the effect is small as photons decouple before Rayleigh scattering is important. At higher frequencies, the visibility function is shifted to lower redshifts where Silk damping is more important. This change in the damping factor produces a proportional change in the multipole spectrum at  $l \sim 6000k$ . The right panels in Figures 3 and 4 show the amplitude of the changes produced by this effect.

### 3.2. Frequency Dependent Surface of Last Scattering

Since the photon cross-section is frequency-dependent, the location of the surface of last scattering will depend on frequency. Since photons emitted at lower redshift are emitted from regions with significant amounts of Silk damping, they contribute little to the observed temperature fluctuations. Because of this latter effect, the surface of last scattering is also  $k$  dependent:

$$\langle 1 + z(k, \nu) \rangle = D(k, \nu)^{-1} \int_0^{\eta_0} d\eta \frac{a_0}{a} \mathcal{V}(\nu, \eta) \exp \left[ -\frac{k^2}{k_D^2(\eta)} \right]. \quad (21)$$

### 3.3. Frequency Dependent Acoustic Wave Phase

Including Rayleigh scattering, the sound horizon at the last scattering  $r_s^{RS+T}[\eta_*(k, \nu)] = \int_0^{\eta_*(k, \nu)} c_s d\eta$  will be frequency dependent. The higher the frequency, the farther the sound horizon. It will shift the peak location by  $\delta k/k(\nu) = 1 - r_s^{RS+T}(\eta_*)/r_s^T(\eta_*)$ , where the superscripts  $^{RS+T}$  and  $T$  stand for the cases with and without Rayleigh scattering respectively. Thus, the peaks in anisotropy spectra will shift in the direction of decreasing  $l$ :  $\delta l/l = \delta k/k$  and  $\frac{\delta C_l}{C_l} = \frac{\partial \ln C_l}{\partial \ln l} \frac{\delta l}{l}$ . The higher the frequencies are, the more the peaks shift.

### 3.4. Frequency Dependent Polarization Amplitude

The amplitude of the microwave background polarization is proportional to the photon mean free path at the surface of last scattering (Zaldarriaga 1995). Since the photon mean free path depends upon frequency, the amplitude of the polarization is now frequency dependent:

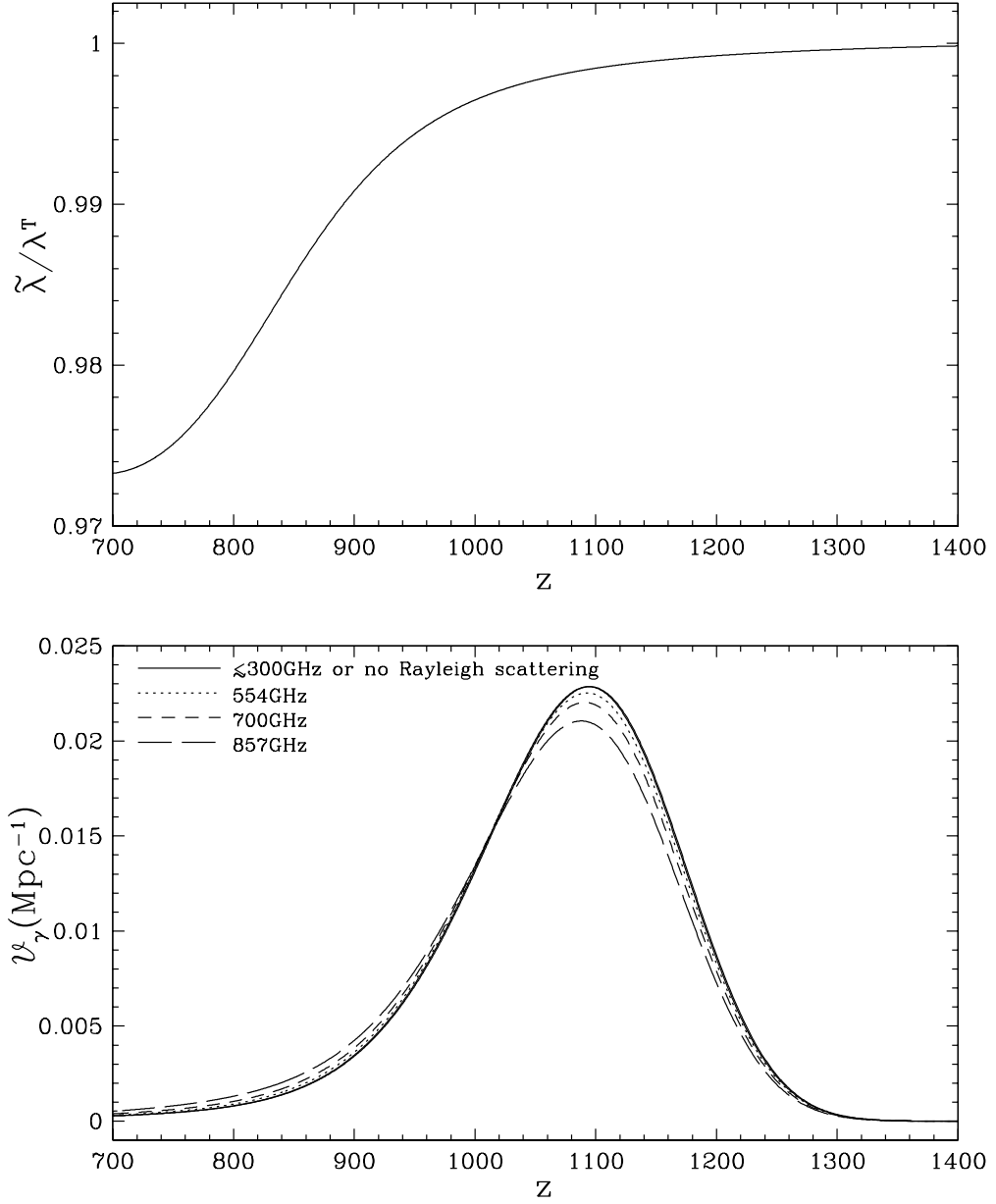


Fig. 1.— The upper panel shows the ratio of the effective photon mean free path with Rayleigh scattering ( $\tilde{\lambda}$ ) to the photon mean free path without Rayleigh scattering ( $\lambda^T$ ). The lower panel shows that the photon visibility function  $V(\nu, \eta)$  shifts toward the present epoch with increasing frequencies.

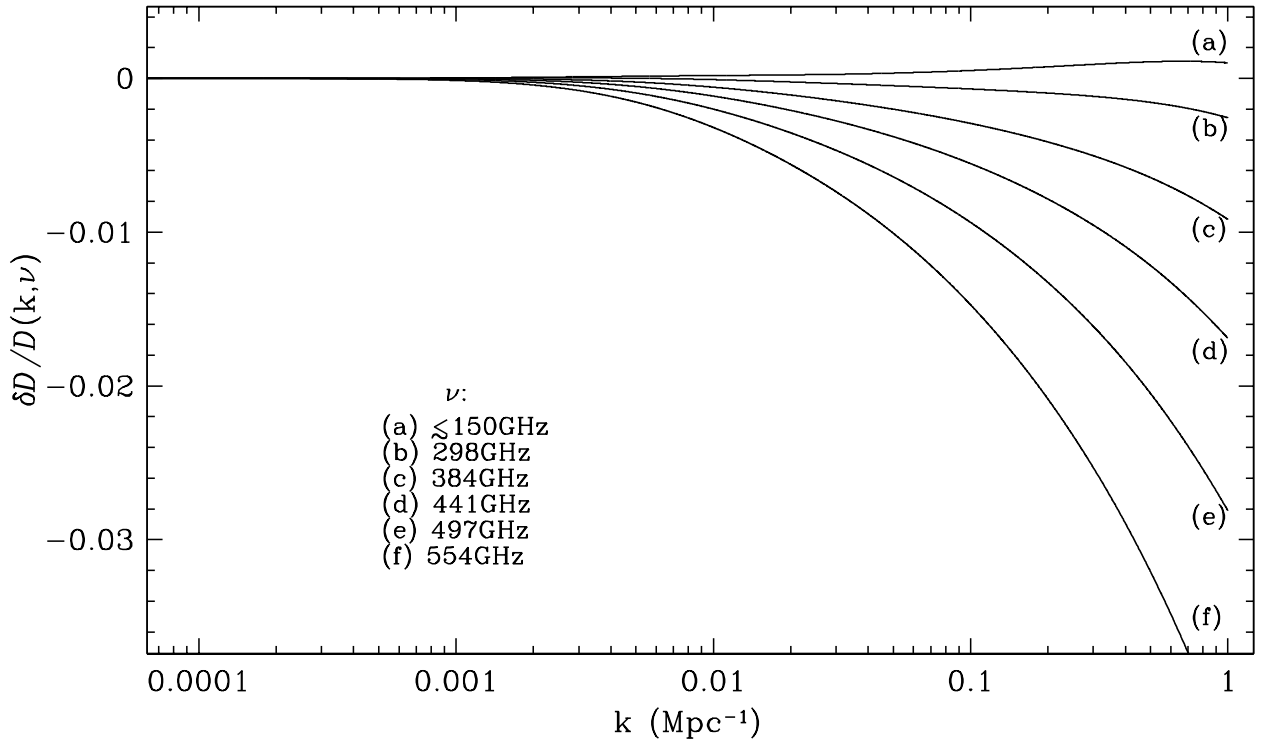


Fig. 2.— Differences of damping factors:  $\delta D/D(k, \nu) = D^{RS+T}(k, \nu)/D^T(k, \nu) - 1$ . The superscripts  $^{RS+T}$  and  $^T$  stand for the cases with and without Rayleigh scattering, respectively. At low frequencies, the increase of  $D^{RS+T}(k, \nu)$  comes mainly from the decrease of mean photon-diffusion length and the suppression of Silk damping; while at high frequencies, the decrease of  $D^{RS+T}(k, \nu)$  is mainly caused by the shift of visibility functions.

$$P(k, \nu) \propto \langle \lambda(\nu, \eta) \rangle = D(k, \nu)^{-1} \int_0^{\eta_0} d\eta \mathcal{V}(\nu, \eta) \exp \left[ -\frac{k^2}{k_D^2(\eta)} \right] \lambda(\nu, \eta). \quad (22)$$

In equation (22), we have weighted the photon mean free path by the visibility function.

#### 4. Numerical Integration

In this section, we describe results of numerical simulations of the full Boltzmann equations. We have revised the CMBFAST<sup>4</sup> code (Seljak & Zaldarriaga 1996) so that it can evolve the Boltzmann equations for frequency dependent scattering. The photon distribution function is approximated by 50 different bins. The fluctuations at each frequency are evolved through the hierarchy of coupled equations (Wilson & Silk 1981; Bond & Efstathiou 1984; Seljak & Zaldarriaga 1996):

$$\dot{\Delta}_{T0,j}^{(S)} = -k\Delta_{T1,j}^{(S)} + \dot{\phi}, \quad (23)$$

$$\dot{\Delta}_{T1,j}^{(S)} = \frac{k}{3} \left[ \Delta_{T0,j}^{(S)} - 2\Delta_{T2,j}^{(S)} + \psi \right] + \dot{\kappa}_j \left( \frac{v_b}{3} - \Delta_{T1,j}^{(S)} \right), \quad (24)$$

$$\dot{\Delta}_{T2,j}^{(S)} = \frac{k}{5} \left[ 2\Delta_{T1,j}^{(S)} - 3\Delta_{T3,j}^{(S)} \right] + \dot{\kappa}_j \left[ \frac{\Pi}{10} - \Delta_{T2,j}^{(S)} \right], \quad (25)$$

$$\dot{\Delta}_{Tl,j}^{(S)} = \frac{k}{2l+1} \left[ l\Delta_{T(l-1),j}^{(S)} - (l+1)\Delta_{T(l+1),j}^{(S)} \right] - \dot{\kappa}_j \Delta_{Tl,j}^{(S)}, \quad \text{for } l > 2, \quad (26)$$

where  $\dot{\kappa}_j$  ( $= -\dot{\tau}$ ) is the (now frequency dependent) differential optical depth and  $\Delta_{Tl,j}$  ( $= \Theta_l(\nu_j, k)/(-i)^l, l \geq 0$ ) is the  $l$ -th multipole moment of the temperature perturbation at frequency  $\nu_j$ . All other symbols and equations (e.g.  $\phi = -\Phi$ ,  $\psi = \Psi$  and  $v_b = -iu_b$ ) are as defined in Seljak & Zaldarriaga (1996).

For the baryons, the momentum equation is now modified to include the frequency-dependent coupling to the photons: in Seljak & Zaldarriaga (1996) is modified:

$$\dot{v}_b = \frac{-\dot{a}}{a} v_b + c_b^2 k \delta_b + \frac{4}{3\rho_b} \sum_j f_j \dot{\kappa}_j (3\Delta_{T1,j}^{(S)} - v_b) + k\psi, \quad (27)$$

where  $f_j$  is the weight per bin. These modifications significantly slow CMBFAST, since it now has to evolve 50 times more variables. We have confirmed that this modified code reproduces standard results.

---

<sup>4</sup>CMBFAST is available at: <http://physics.nyu.edu/matiasz/CMBFAST/cmbfast.html>.

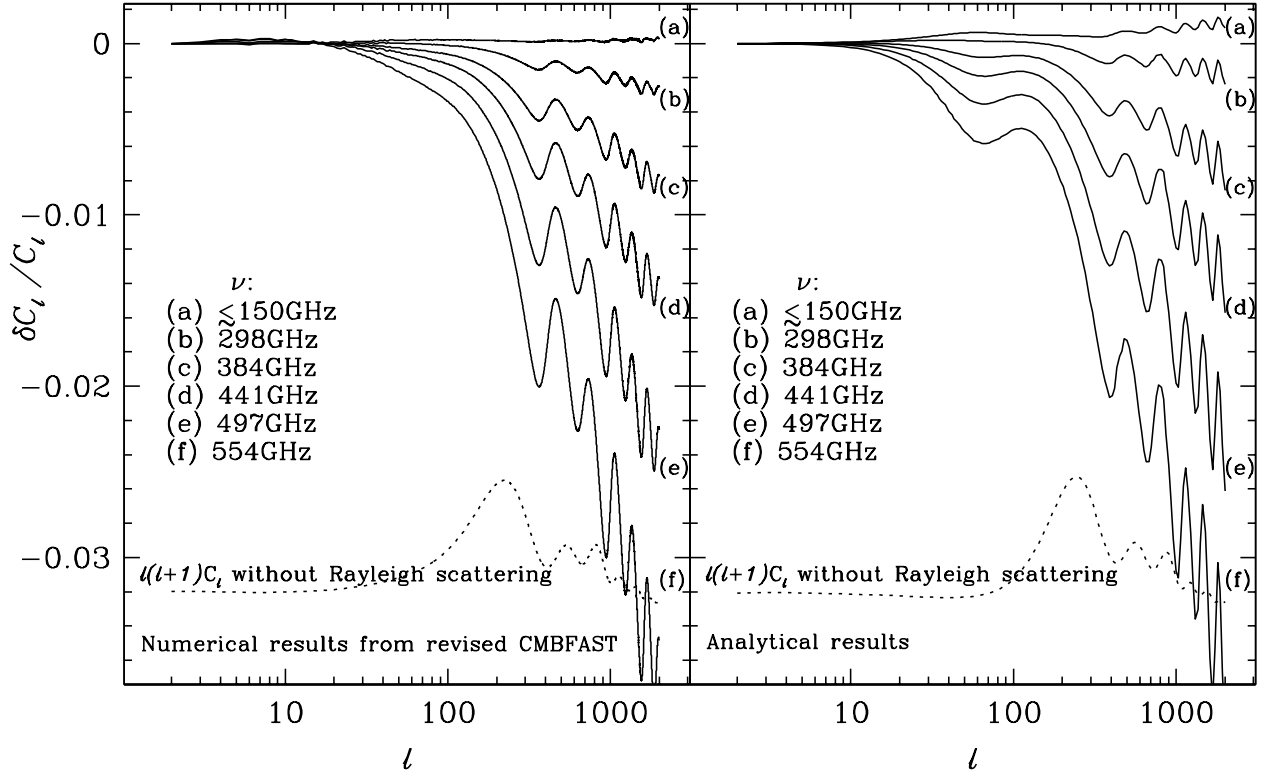


Fig. 3.— Relative differences of anisotropy spectra with and without Rayleigh scattering:  $\delta C_l / C_l(\nu) = C_l^{RS+T}(\nu) / C_l^T - 1$  (solid curves). Basically, they keep the forms of their damping factor differences (see Fig. 2). The dotted curves represent the power spectra  $l(l+1)C_l$  without Rayleigh scattering (in arbitrary unit). The oscillations of  $\delta C_l / C_l$  show that the power spectra with Rayleigh scattering shift in the direction of decreasing  $l$ . The higher the frequencies are, the more the spectra shift (higher oscillation peak height). Note that the peak locations are not exactly same in the numerical results and in the analytical results.

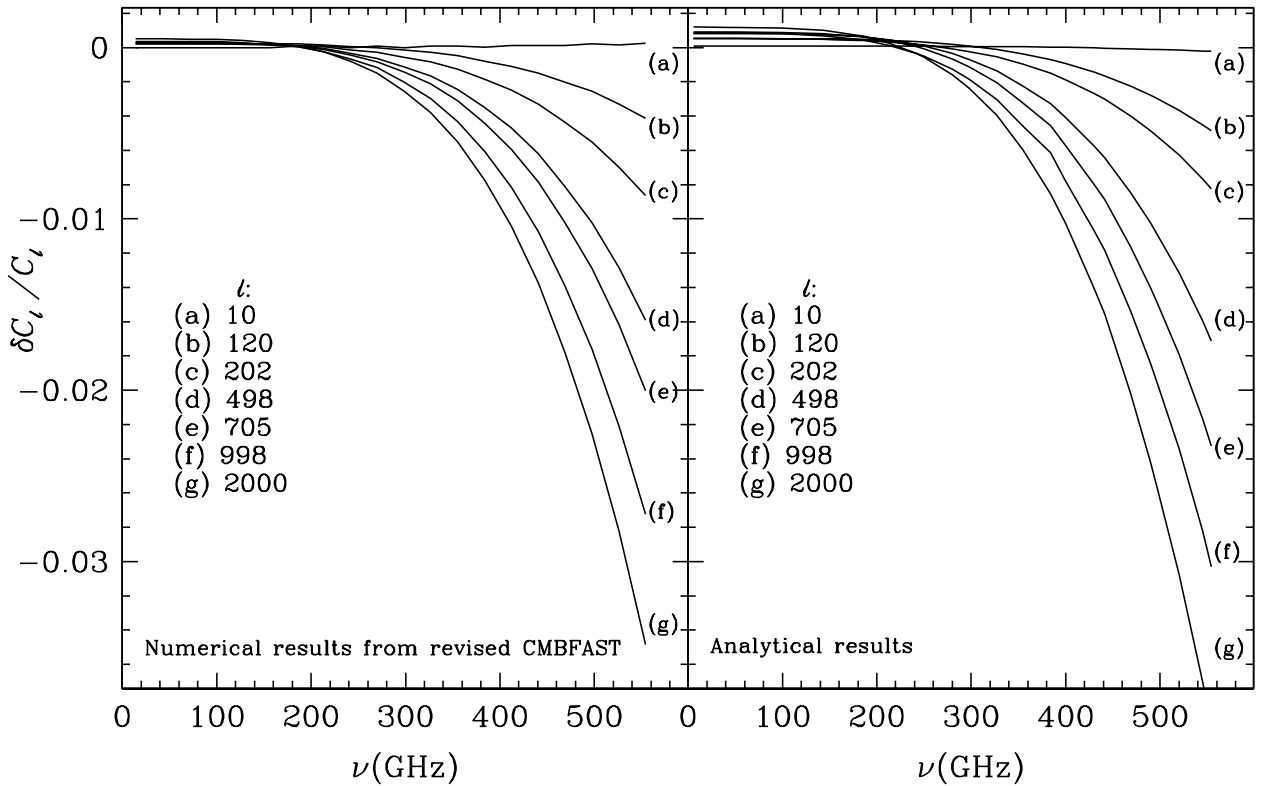


Fig. 4.— Relative differences of anisotropy spectra with and without Rayleigh scattering:  $\delta C_l/C_l(\nu) = C_l^{RS+T}(\nu)/C_l^T - 1$ . The positive differences at low frequencies come from the decrease of mean photon-diffusion length. The differences between the numerical results and the analytical results are partly caused by slightly different peak locations (see Fig. 3).

In our numerical calculations, we use the recombination results of  $n_e$  and  $n_H$  from RECFAST code to calculate the opacity to photon propagation (Seager, Sasselov & Scott 1999).

Our numerical calculations agree remarkably well with the analytical estimates of (§2). Figures 3 and 4 show their relative differences as a function of  $l$  and  $\nu$ . As seen from the figures, the analytical results are qualitatively consistent with the numerical results. At high multipoles and high frequencies, the anisotropy spectra in both results decrease because the visibility functions shift to lower redshifts where Silk damping is more important. The effect is up to 0.5% for  $\nu \sim 350\text{GHz}$  and 3% for  $\nu \sim 550\text{GHz}$  at  $l \sim 1000$ . At low frequencies and high multipoles, both the analytical and numerical results show that the anisotropy spectra with Rayleigh scattering are higher ( $\sim 0.1\%$ ) than the spectrum without Rayleigh scattering, which is caused by the increase of damping factor  $D(k, \nu)$  at low frequencies (Fig.2). At low  $l$ , that difference is too small to be physically significant because the cosmic variance uncertainty is comparably too large ( $\sim 10\%$  for  $l < 10$ ). In Fig.3, comparing to the peaks of the anisotropy spectrum without Rayleigh scattering, all the oscillation peaks of the spectrum differences shift  $\sim 1/4$  “period” in the direction of decreasing  $l$ , which supports our analyses about the phase shift caused by frequency-dependent sound horizons at the last scattering in §3.3. The oscillation amplitude of the spectrum difference is up to 0.5% at  $\nu \sim 550\text{GHz}$  and  $l \sim 1000$ .

There are small difference between the numerical calculations and our analytical estimates. Note that the shift of the first peak is more evident in the analytical results. These differences may be due to the assumption that  $\hat{\Theta}_0$ ,  $\hat{\Theta}_1$  and the potential are not affected by Rayleigh scattering, or they may be due to using equation (16) rather than the exact solution of equation (15).

## 5. Discussion and Conclusion

In this paper, we estimate the effects of Rayleigh scattering on the microwave background. For *MAP*, Rayleigh scattering is a relatively minor correction. The largest effect is that it reduces the amount of Silk damping by  $\sim 0.1\%$  at  $\nu \sim 100\text{GHz}$  and  $l \sim 1000$ . The systematic error is comparable to *MAP*’s statistical errors. For the *Planck Surveyor*’s highest frequencies, Rayleigh scattering can have significant effects on the shape and amplitude of the microwave background fluctuation spectrum. Overall, it reduces amplitudes,  $C_l$ , increasingly with increasing multipole number  $l$ , and, for observations at a single frequency, might be confounded with varying  $\Omega_b h^2$ . However the frequency dependence of Rayleigh scattering imparts a distinctive signature, so that the effects pointed at in this paper should

be easily corrected. At  $\sim 550$  GHz, the anisotropy spectrum decreases as much as 3%. The peak shift between the spectra of 100 and 500GHz makes their relative difference oscillate as a function of  $l$ . The oscillation amplitude is as high as 0.5%, much larger than the statistical uncertainties in the *Planck Surveyor* data. While the high-frequency channels with  $\nu > 353$ GHz are going to be used primarily for dust modeling, it is useful to note that the cosmic microwave background fluctuations will not be frequency independent. By looking at regions of low dust emission, the *Planck Surveyor* should be able to detect this effect. This detection would be an additional check of the recombination history of the universe, and a direct measurement of the formation of atoms in the early universe.

## 6. Acknowledgements

We thank Wayne Hu, Arthur Kosowsky, Sarah Seager and Matias Zaldarriaga for useful discussions. We thank Uros Seljak and Matias Zaldarriaga for the use of the CMBFAST code. We thank Bruce Draine for pointing out an error in an early manuscript and leading us to the correction. DNS is supported in part by the *MAP* program.

## REFERENCES

Bond, J. R., & Efstathiou, G. 1984, ApJ, 285, L45

Dodelson, S., & Jubas, J. M. 1995, ApJ, 439, 503

Gnedin, N.Y., & Gnedin, O.Y. 1998, ApJ, 509, 11

Hannestad, S. 2001, New Astronomy, 6, 17

Hu, W., Scott, D., Sugiyama, N., & White, M. 1995, Phys. Rev. D, 52, 5498

Hu, W., & Sugiyama, N. 1995, ApJ, 444, 489

Hu, W., & Sugiyama, N. 1996, ApJ, 471, 542

Lang, K. R. 1999, in *Astrophysical Formulae* (New York: Springer)

Peebles, P. J. E. 1980, *Large Scale Structure*, (Princeton University Press: Princeton, NJ 08540)

Peebles, P. J. E., & Yu, J. T. 1970, ApJ, 12, 815

Seager, S., Sasselov, D. D., & Scott, D. 1999, ApJ, 523, L1

Seljak, U., & Zaldarriaga, M. 1996, ApJ, 469, 437

Stancil, P. C., Lepp, S., & Dalgarno, A. 1998, ApJ, 509, 1

Wilson, M. L., & Silk, J. 1981, ApJ, 243, 14

Zaldarriaga, M., & Harari, D. D. 1995, Phys. Rev. D 52, 3276